International Conference on Nuclear Data for Science and Technology 2007
DOI: 10.1051/ndata:07497

Photonuclear data evaluations of actinides up to 130 MeV

E. Dupont[1,a], I. Raškinytė[1], A.J. Koning[2], and D. Ridikas[1]

[1] CEA Saclay, DSM/DAPNIA/SPhN, 91191 Gif-sur-Yvette, France
[2] NRG Petten, P.O. Box 25, 1755 ZG Petten, The Netherlands

Abstract. There is a renewed interest in photonuclear reactions for various applications such as active nuclear material detection techniques and radioactive ion beam or neutron production targets. However, contrary to the neutron induced reactions, evaluated nuclear data libraries contain little information for photons. In particular, there are very few photonuclear data evaluations of actinides above 20 MeV. This paper gives an overview of our on-going activities on photonuclear data evaluation of actinides up to 130 MeV.

1 Introduction

Nuclear data of photo-induced reactions are important for a variety of existing or emerging applications. Among them are radiation transport simulation and radiation shielding design of accelerators or innovative reactors, activation analysis, safeguards and inspection technologies. In terms of incident energies, the giant dipole resonance (GDR) region below 30 MeV is essential for most applications. However, photonuclear data up to 130 MeV are also necessary for the simulation of intense neutron sources and to complement the neutron and proton high-energy libraries.

Actinide cross section evaluations were reviewed in the framework of a specific IAEA coordinated research project [1]. Recently, major actinide cross sections and spectra were evaluated in the framework of a collaboration between LANL and CEA [2]. These evaluations were done for incident photon energies below 20 MeV. To our knowledge, ^{235}U, ^{238}U, and ^{237}Np from the JENDL Photonuclear Data File [3] are the only actinide evaluations available above 20 MeV.

The present work aims at the extension of actinide evaluations up to 130 MeV. This paper presents on-going evaluation activity for ^{232}Th [4], ^{235}U [4,5], ^{238}U, and ^{239}Pu [6]. Recent measurements of delayed neutron yields performed at CEA [7,8] will complement this evaluation effort and the outcome will be proposed for insertion into the Joint Evaluated Fission and Fusion (JEFF) library to respond to application needs.

2 Photonuclear reactions

In a photoreaction, the target nucleus is directly excited by the incident photon. Below a few tens of MeV, the main decay channels are neutron emission and fission only, because of the high Coulomb barrier of heavy nuclei. However, light charged particle emission may become significant at higher energies.

In this work, the photoabsorption process is described by the GDR and quasideuteron mechanisms. The preequilibrium step of particle emission is treated with the classical exciton model. At equilibrium, the compound nucleus decay channels are handled within the Hauser-Feshbach statistical formalism. Neutron transmission coefficients in the exit channel are calculated with a global deformed optical model potential (OMP) developed for neutron-actinide interaction. Finally, the transmission coefficients through fission barriers, described by inverted parabola, are calculated within the fission channels theory of Bohr.

These calculations are performed using one single code, TALYS [9], to model in a consistent way the reaction cross sections, particle energy spectra, and residual production cross sections of all open channels up to 130 MeV.

2.1 Photoabsorption

At low energies, below about 30 MeV, the GDR is the dominant excitation mechanism. At higher energies, up to the pion threshold (about 140 MeV), the phenomenological model of photoabsorption on a neutron-proton pair (quasideuteron, QD) becomes dominant. The photoabsorption cross section is the sum of these two components.

The GDR component of deformed nuclei, such as actinides, is given as a sum of two Lorentzians

$$\sigma_{GDR}(E_\gamma) = \sum_{i=1,2} \sigma_{E1,i} \frac{E_\gamma^2 \Gamma_{E1,i}^2}{(E_\gamma^2 - E_{E1,i}^2)^2 + E_\gamma^2 \Gamma_{E1,i}^2}, \qquad (1)$$

where $\sigma_{E1,i}$, $E_{E1,i}$, $\Gamma_{E1,i}$ are the GDR peak cross section, energy position and width respectively.

The QD component relates the photoabsorption cross section to the experimental deuteron photodisintegration cross section $\sigma_d(E_\gamma)$

$$\sigma_{QD}(E_\gamma) = \frac{L}{A} NZ \sigma_d(E_\gamma) f(E_\gamma), \qquad (2)$$

where L is the Levinger parameter [10] and $f(E_\gamma)$ is the Pauli-blocking function [11].

2.2 Nucleus decay

In the statistical approach, the competition between all decay channels involves major ingredients such as nuclear level

[a] Presenting author, e-mail: emmeric.dupont@cea.fr

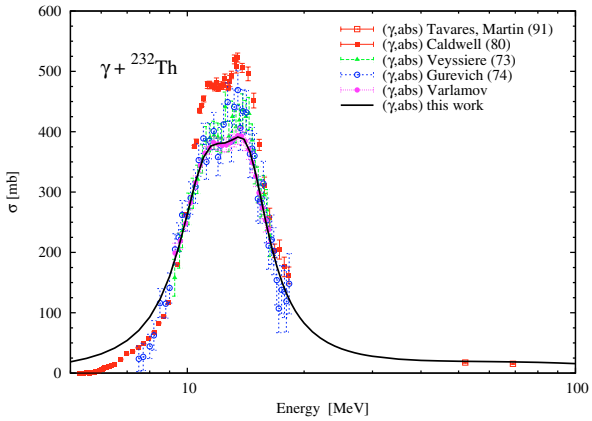

Fig. 1. Modelling of ^{232}Th photoabsorption cross section.

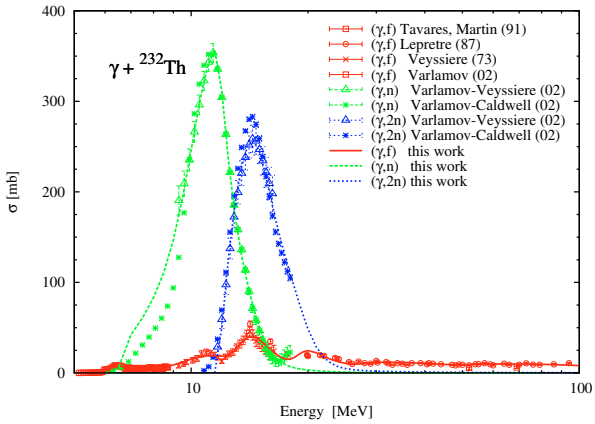

Fig. 2. Modelling of ^{232}Th (γ,n), (γ,2n) and (γ,f) cross sections.

density and transmission coefficients through optical potential or fission barrier. The nuclear level density is modelled using the Gilbert-Cameron composite formula [12] with an energy-dependent level density parameter [13]. The following paragraphs shortly describe the main models used to calculate neutron and fission transmission coefficients.

2.2.1 Neutron emission

Assuming time-reversal invariance of nuclear reactions, the exit channel in the (γ,n) reaction shares the same nuclear parameters as the entrance channel of the (n,γ) reaction. Therefore, neutron transmission coefficients for the exit channel are calculated with a global coupled-channels optical potential developed for neutron-actinide interaction up to 200 MeV by Soukhovitskii [14]. In the latter work, the optical potential parameters were adjusted to reproduce available neutron- and proton-induced cross sections on ^{238}U and ^{232}Th targets. This global potential together with local deformation parameters was used to calculate neutron transmission coefficients.

2.2.2 Fission channel

In this work, fission barriers are described by a double humped barrier model for all nuclei. One assumes that tunnelling through two barriers A and B can be separated into two steps, and the effective fission transmission coefficient is given by

$$T_{eff} = T_A \frac{T_B}{T_A + T_B}. \quad (3)$$

According to the fission channels theory of Bohr, the total fission transmission coefficient is the sum of the individual transmission coefficients for each transition state through which the nucleus may tunnel. The individual transmission coefficients are calculated using the Hill-Wheeler expression

$$T_{HW}(E) = \left[1 + exp\left(-2\pi \frac{E - B_f}{\hbar\omega}\right)\right]^{-1}, \quad (4)$$

where B_f is the barrier height relative to the nucleus ground state and $\hbar\omega$ is the barrier curvature. Those barrier parameters are adjusted to reproduce the experimental cross sections.

3 Calculations and results

The TALYS code contains models for comprehensive nuclear reaction calculations. The version TALYS-0.72 [15] of this code is used to reproduce the data available in the EXFOR database [16] and to fill any experimental gap with model predictions up to 130 MeV.

3.1 Thorium-232

Photoabsorption. A recent review of photoneutron emission measurements made by Varlamov [17] shows systematic discrepancies between Livermore [18] and Saclay [19] experimental data. In the present work, the ^{232}Th GDR parameters were adjusted to reproduce the corrected photoabsorption cross section proposed by Varlamov (fig. 1). The same GDR parameters were assumed for the ^{231}Th and ^{230}Th isotopes since no experimental data could be found.

Neutron emission. In the present calculations we have only used the first three states of the ground state rotational band together with unaltered optical potential parameters from Soukhovitskii [14]. In addition ^{231}Th + neutron transmission coefficients have also been used for ^{230}Th + neutron exit channel. The influence of these approximations on (γ,n), (γ,2n) and (γ,f) cross sections is negligible. The quadrupolar and hexadecapolar deformation parameters published by Soukhovitskii for ^{232}Th have been used for ^{231}Th and ^{230}Th also. In addition, the default normalization of the matrix element in TALYS exciton model was fine-tuned to better reproduce the experimental data (fig. 2).

Photofission. There are experimental evidences that the fission barrier of thorium isotopes is more complex than for uranium or plutonium isotopes. However, we have approximated the fission barriers with a double-humped barrier and ignore the splitting of the outer barrier. Nevertheless, the experimental ^{232}Th photofission cross section was rather well reproduced as shown in figure 3 which compares the calculated fission cross sections with measurements. The presence of a peak in the fission cross section between 6 and 7 MeV is due to 0^- and 1^- transition states located about half-a-MeV above the second fission barrier of ^{232}Th.

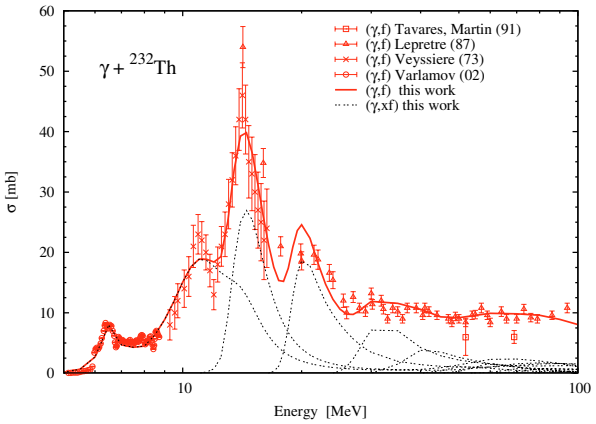

Fig. 3. Details of the ^{232}Th photofission cross section.

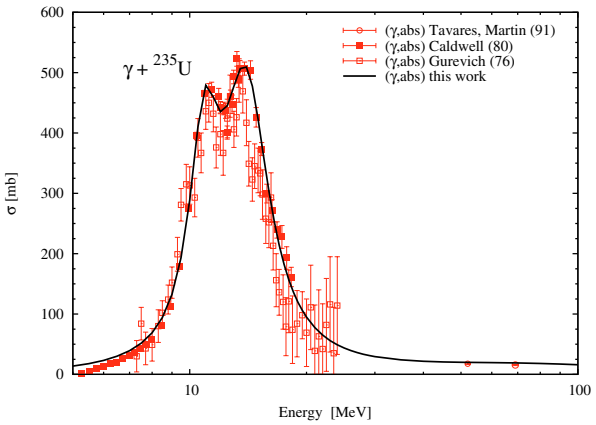

Fig. 4. Modelling of ^{235}U photoabsorption cross section.

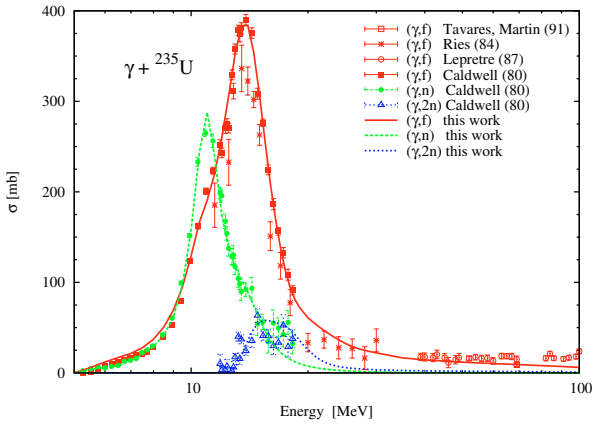

Fig. 5. Modelling of ^{235}U (γ,n), (γ,2n) and (γ,f) cross sections.

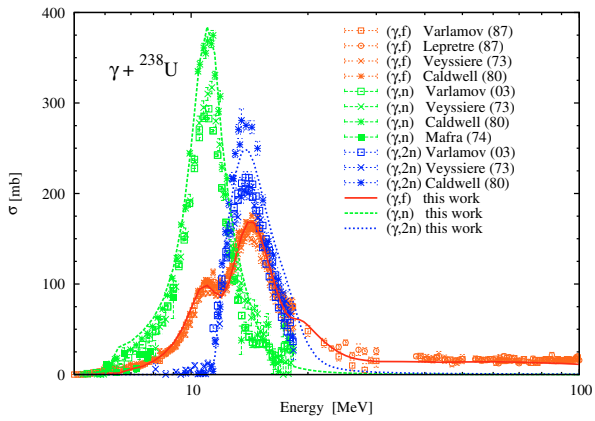

Fig. 6. Modelling of ^{238}U (γ,n), (γ,2n) and (γ,f) cross sections.

3.2 Uranium-235

Photoabsorption. The GDR parameters used in TALYS for uranium isotopes are from RIPL-2 [20]. The latter were adjusted onto experimental data by Caldwell [18]. Figure 4 shows a comparison between TALYS photoabsorption cross section and experimental data. Caldwell points are given as the sum of (γ,n), (γ,2n) and (γ,f) partial cross sections, while Gurevich [21] directly measured the total photoabsorption cross section.

Neutron emission. The neutron transmission coefficients for the ^{234}U + n exit channel were calculated with the global deformed OMP by Soukhovitskii [14] using the same approximation than in the ^{232}Th case. For the ^{234}U deformation parameters, we have used interpolated values between ^{233}U and ^{235}U parameters given in the reference [14]. The emission of photoneutrons above 12 MeV was further improved by adjusting the preequilibrium normalization constant (fig. 5).

Photofission. A number of calculations were done in order to find a set of fission barrier parameters which reproduce Caldwell [18] experimental data (fig. 5).

3.3 Uranium-238

Photoabsorption. This cross section is calculated using GDR parameters from RIPL-2 [20]. As for ^{235}U, the latter were adjusted to reproduce Caldwell measurements [18].

Neutron emission. All neutron transmission coefficients are calculated with Soukhovitskii global OMP using deformation parameters published in the reference [14]. Figure 6 shows that (γ,n) cross section is in good agreement with Caldwell measurement, which is a consequence of the GDR parameters choice. However, present results overestimate both Veyssiere [19] and Varlamov [17] data. New calculations using GDR parameters based on recommended data proposed by Varlamov are being performed.

Photofission. Starting from RIPL-2 fission barrier parameters, several iterations were necessary in order to reach an optimal reproduction of the experimental photofission cross sections (fig. 6).

3.4 Plutonium-239

Photoabsorption. Gurevich [21] and de Moraes [22] directly measured the photoabsorption cross section, whereas Berman [23] measured the main partial cross sections. Their sum also gives the total photoabsorption cross section. To be consistent with partial cross sections modelling, present GDR parameters are fitted on Berman data (fig. 7).

Neutron emission. To model the inverse ^{238}Pu + neutron channel we used the Soukhovitskii global OMP together with deformation parameters given in the reference [14] for the

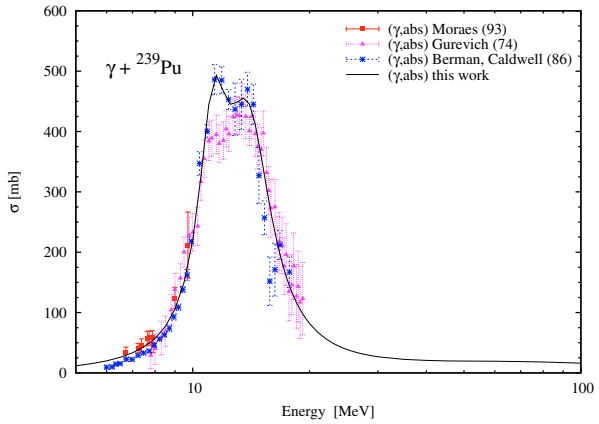

Fig. 7. Modelling of ^{239}Pu photoabsorption cross section.

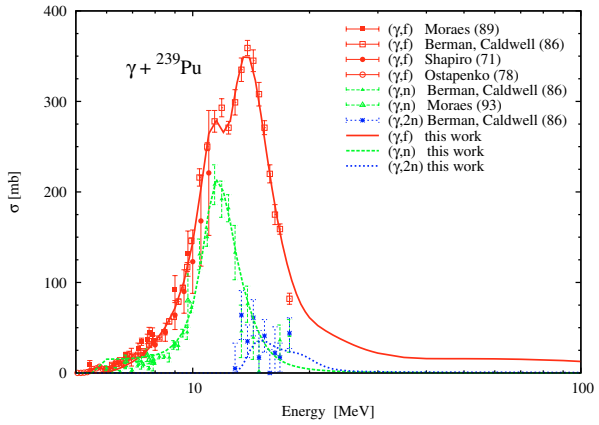

Fig. 8. Modelling of ^{239}Pu (γ,n), (γ,2n) and (γ,f) cross sections.

^{239}Pu nucleus. The same neutron transmission coefficients are used for the ^{237}Pu + neutron $(\gamma, 2n)$ exit channel. Results are displayed on figure 8.

Photofission. Figure 8 also shows a comparison of present calculations with experimental photofission data. Slight adjustments in fission barrier parameters were necessary to improve the agreement between calculation and measurements.

4 From calculation to evaluations

The present results are being converted into the ENDF-6 format thanks to TALYS/TEFAL formatting capabilities [24] and processed with the standard utility codes to check conformity with ENDF rules and procedures. As a final test, these evaluations will be processed through NJOY to build new MCNP(X) files and allow further validation of the quality of the data.

5 Conclusion and outlook

Photonuclear cross sections up to 130 MeV were calculated with the latest version of the TALYS code using a deformed optical potential by Soukhovitskii to model the neutron emission. The fission transmission coefficients were calculated using a double humped barrier model. Fission barriers heights and widths were adjusted in order to reproduce experimental data. Complete evaluated files will be available shortly for ^{232}Th, ^{235}U, ^{238}U and ^{239}Pu. These files will be proposed for insertion into the Joint Evaluated Fission and Fusion (JEFF) library to respond to application needs up to 130 MeV.

References

1. *Handbook on photonuclear data for applications – Cross sections and spectra*, IAEA Report, TECDOC-1178, 2000.
2. M.-L. Giacri-Mauborgne et al., Nucl. Sci. Eng. **153**, 33 (2006).
3. N. Kishida et al., *Proc. of the Int. Conf. on Nuclear Data for Science and Technology, Santa Fe, USA, 2004*.
4. I. Raškinytė et al., *Proc. of the Int. Conf. on Nuclear Reaction Mechanisms, Varenna, Italy, 2006.*
5. I. Raškinytė, E. Dupont, D. Ridikas, *Photonuclear Data Evaluation of* ^{235}U, JEFF Meeting, November 2005, JEF/DOC-1117, and CEA Saclay Report DAPNIA-06-101.
6. I. Raškinytė, E. Dupont, D. Ridikas, *Photonuclear Data Evaluation of* ^{239}Pu, CEA Saclay Report, DAPNIA-06-318, 2006.
7. A. Van Lauwe et al., *Proc. of the Int. Conf. on Nuclear Reaction Mechanisms, Varenna, Italy, 2006*.
8. D. Doré et al., *Delayed neutron yields and time spectra from photofission of actinides* (these proceedings).
9. A. Koning, S. Hilaire, M.C. Duijvestijn, *TALYS-1.0* (these proceedings).
10. J.S. Levinger, Phys. Rev. **84**, 43 (1951).
11. M.B. Chadwick et al., Phys. Rev. C **44**, 814 (1991).
12. A. Gilbert, A.G.W. Cameron, Can. J. Phys. **43**, 1446 (1965).
13. A.V. Ignatyuk, G.N. Smirenkin, A.S. Tishin, Sov. J. Nucl. Phys. **21**, 255 (1975).
14. E.Sh. Soukhovitskii et al., J. Phys. G Nucl. Part. Phys. **30**, 905 (2004).
15. A. Koning, S. Hilaire, M. Duijvestijn, *TALYS-0.72 – User manual*, NRG Report, December 2006.
16. Nuclear Reaction Data Centres Network (NRDC, IAEA), cf. http://www-nds.iaea.org/
17. V.V. Varlamov et al., *Consistent evaluation of photoneutron reaction cross sections using data obtained [...] at Livermore and Saclay*, IAEA Report, INDC(CCP)-440, 2004, p. 37.
18. J.T. Caldwell et al., Phys. Rev. C **21**, 1215 (1980).
19. A. Veyssiere et al., Nucl. Phys. A **199**, 45 (1973).
20. *Handbook for calculations of nuclear reaction data, RIPL-2*, IAEA report, TECDOC-1506, 2006.
21. G.M. Gurevich et al., Nucl. Phys. A **273**, 326 (1976).
22. M.A. de Moraes, M.F. Cesar, Physica Scripta **47**, 519 (1993).
23. B.L. Berman et al., Phys. Rev. C **34**, 2201 (1986).
24. A. Koning, *Creating ENDF-6 files with TALYS*, NRG Report, January 2007 (unpublished).